Conf-931079--13

BIAXIAL LOADING AND SHALLOW-FLAW EFFECTS ON CRACK-TIP CONSTRAINT AND FRACTURE-TOUGHNESS

W. E. Pennell, B. R. Bass, J. W. Bryson, W. J. McAfee,
T. J. Theiss, and M. C. Rao

Heavy-Section Steel Technology Program
Oak Ridge National Laboratory
Oak Ridge, Tennessee 37831

DISCLAIMER

Biaxial Loading and Shallow-Flaw Effects on Crack-Tip Constraint and Fracture-Toughness*

W. E. Pennell,† B. R. Bass,** J. W. Bryson,† W. J. McAfee,†
T. J. Theiss,† and M. C. Rao‡

Oak Ridge National Laboratory

Abstract

Uniaxial tests of single-edged notched bend (SENB) specimens with both deep- and shallow-flaws have shown elevated fracture-toughness for the shallow flaws. The elevation in fracture-toughness for shallow flaws has been shown to be the result of reduced constraint at the crack-tip. Biaxial loading has the potential to increase constraint at the crack-tip and thereby reduce some of the shallow-flaw, fracture-toughness elevation. Biaxial fracture-toughness tests have shown that the shallow-flaw, fracture-toughness elevation is reduced but not eliminated by biaxial loading. Dual-parameter, fracture-toughness correlations have been proposed to reflect the effect of crack-tip constraint on fracture-toughness. Test results from the uniaxial and biaxial tests were analyzed using the dual-parameter technology. Discrepancies between analysis results and cleavage initiation site data from fractographic examinations indicate that the analysis models are in need of further refinement. Addition of a precleavage, ductile-tearing element to the analysis model has the potential to resolve the noted discrepancies.

Introduction

Fracture mechanics technology is used to assess the structural integrity of irradiation-embrittled reactor pressure vessels (RPV's) containing flaws. The fracture mechanics technology currently in use is based upon analysis methods and fracture-toughness data appropriate for cracks with a high degree of crack-tip constraint. This approach has the advantage that it produces very conservative estimates of allowable RPV operating conditions, and therefore assures high levels of safety. There is a concern, however, that the level of conservatism inherent in the limiting crack-tip constraint approach to RPV safety assessment may have economically unacceptable consequences when applied to configurations and loading conditions where upper-bound levels of crack-tip constraint do not exist.

In part, the current approach to the structural integrity assessment of irradiation-embrittled RPV's stems from limitations of the nondestructive examination (NDE) technology available at the time the fracture mechanics technology was developed. Substantial advances in NDE technology have been made since that time. Detection and accurate sizing of relatively small flaws is now possible. Conceptually it is now possible to define requirements for the fracture analysis of RPVs in terms of the flaws detected and sized during in-service NDE examinations. For this approach to become a practical reality, however, fracture mechanics technology appropriate to these new conditions must be developed and validated.

---

*Research sponsored by Division of Engineering, Office of Nuclear Regulatory Research, U.S. Nuclear Regulatory Commission under Interagency Agreement 1886-8011-9B with the U.S. Department of Energy under contract DE-AC05-84OR21400 with Martin Marietta Energy Systems, Inc.

†Engineering Technology Division.

**Computing Applications Division.

‡Consultant to the Metals and Ceramics Division.

Features of the flaws of interest in an NDE based RPV safety assessment are that they are relatively shallow and located in a biaxial stress field. Fracture technology advances required to address these conditions include the development of a fracture-toughness data base for shallow flaws and determination of the effect of biaxial stress fields on the shallow-flaw, fracture-toughness. Shallow-flaw, fracture-toughness would be expected to be higher than the deep-flaw fracture toughness currently in use because of the proximity of the vessel inner surface to the crack-tip and the consequent decrease in crack-tip constraint. Biaxial loading would act to restore some of the crack-tip constraint and reduce, but not eliminate, some of the fracture-toughness elevation associated with shallow flaws.

Development of analysis techniques which adequately reflect the effects of crack-tip constraint on fracture-toughness is clearly essential to the implementation of an advanced fracture analysis technology. Development of fast and economical high-volume computing capabilities has made possible the detailed analysis of the elastic-plastic stress fields at the crack-tip. Crack-tip constraint can, therefore, be characterized in terms of its effect on the crack-tip stress fields. Dual-parameter, fracture-toughness correlations and corrections have been proposed for this purpose. Refining and validating these dual-parameter fracture analysis methods is an important element of an advanced fracture technology development program.

The above discussion of the use for an advanced fracture mechanics technology has been in terms of its application to the evaluation of flaws discovered and characterized during an in-service NDE examination. It should be noted, however, that other important RPV safety assessment applications exist. These include (a) the probabilistic fracture mechanics analysis of reactor pressure vessel integrity under postulated pressurized thermal shock (PTS) transient loading, and (b) transfer of data from future miniature fracture mechanics RPV surveillance specimens for application to RPV safety assessments.

The Nuclear Regulatory Commission (NRC) sponsored Heavy-Section Steel Technology (HSST) Program at Oak Ridge National Laboratory (ORNL) is conducting research to generate the fracture-toughness data to develop and validate the analysis methods required for the application of an advanced fracture mechanics technology to RPV safety assessments. This paper provides an interim report of results from that research.

Constraint Effects In Fracture

Fracture occurs when the opening mode tensile stresses at the tip of a crack in a brittle material exceed a critical value over a finite length (1). Local yielding of the material at the crack-tip limits the buildup of opening-mode stresses and thereby directly influences fracture-toughness.

Crack-tip stress fields can be divided into hydrostatic and shear components. Yielding of the material is governed by the shear component of the stress field. Tensile hydrostatic stresses contribute directly to the crack-tip opening mode tensile stresses but do not influence yielding. It follows, therefore, that fracture-toughness will be directly influenced when the hydrostatic component of the crack-tip stress field increases.

Crack-tip constraint is the term used to describe conditions which influence the hydrostatic component of the crack-tip stress field. Low constraint reduces the hydrostatic stress contribution to the opening mode stress and thereby increases the fracture-toughness relative to that obtained in a high-constraint configuration.

Plane strain constraint of a crack embedded in a large elastic body represents what may be a practical upper limit to crack-tip constraint. In such a condition the crack-tip plastic zone is very small when compared with the test specimen dimensions. Irwin (2) demonstrated that fracture-toughness of a material for conditions of linear elastic plane-strain (LEPS) constraint of the crack-tip

plastic zone can be adequately characterized by a single parameter, the stress-intensity factor K_{Ic}. Hutchinson (3), Rice, and Rosengren (4) showed that crack-tip stresses can be uniquely defined for these conditions for a power-law hardening material. The singular crack-tip stress distribution associated with LEPS constraint is designated the HRR stress distribution.

The LEPS crack-tip constraint condition is attractive for fracture-toughness testing because it can be readily reproduced in any testing laboratory. Fracture-toughness testing standards such as the American Society for Testing and Materials (ASTM) Standard E399 (5), therefore, requires that LEPS crack-tip constraint be present in a test specimen for the fracture-toughness test data to be considered valid. Assurance that the required LEPS constraint condition was achieved during a test is obtained by requiring that the test specimen size be not less than a minimum acceptable size governed by the material yield stress and the measured fracture-toughness. The requirements of ASTM E399 have the practical effect of limiting the size of the crack-tip plastic zone radius at fracture to approximately 2% of both the crack-depth and the test specimen thickness.

Fracture-toughness data produced using test specimens with LEPS crack-tip constraint represent what is probably a lower bound fracture-toughness for a material. Test specimen dimensions required for the maintenance of LEPS crack-tip constraint conditions can be very large. Fracture-toughness tests of A533B material conducted at temperatures in the transition range of the fracture-toughness curve required the use of 10T and 12T compact tension (CT) test specimens (6). These test specimens incorporate crack depths of 254 mm (10 in) and 304.8 mm (12 in.), respectively.

Departure from conditions of LEPS crack-tip constraint results in a crack-tip stress distribution which is no longer singular. It differs from the HRR stress distribution in a manner dictated by the crack-tip constraint. This difference directly influences the fracture-toughness associated with a particular material and crack-geometry combination. The fracture-toughness now becomes constraint-dependent. It follows, therefore, that a second parameter must be added to the fracture-toughness characterization to account for the influence of departures from LEPS crack-tip constraint.

Dual-Parameter, Fracture-Toughness Corrections and Correlations

Dual-parameter, fracture-toughness corrections and correlations have been proposed to provide a quantitative assessment of effect of reduction of crack-tip constraint on fracture-toughness. Principal features of the J-Acr fracture-toughness correction proposed by Dodds–Anderson (7), and the J-Q dual-parameter, fracture-toughness correlation proposed by O'Dowd and Shih (8, 9) are illustrated in Fig. 1.

The Dodds–Anderson J-Acr correction factor approach provides a quantitative adjustment for fracture-toughness data when the LEPS constraint conditions associated with valid K_{Ic} data have not been maintained. Formulation of the J-Acr correction factor approach is based upon the following principles and assumptions: (a) initiation of cleavage fracture is governed by a stress-based criterion which remains constant for a range of crack-tip constraint conditions; (b) cleavage initiation occurs in a region of the crack-tip stress field where stresses can be adequately defined using small-scale yielding (SSY) continuum mechanics-based, finite-element analysis models; (c) fracture occurs in two specimens with differing levels of crack-tip constraint when stresses at specific locations on the crack plane ahead of the crack tip reach a common reference value. The reference stress value does not have to be rigorously defined if the crack-tip stress fields are self-similar since the same value will be used in each of the constraint conditions being compared; (d) the specific location (r) along the crack plane selected for assuring equivalence of opening mode stresses is not critical, provided that the location selected is within the zone where SSY continuum mechanics-based analysis models can adequately define the stress field. A value of $r = 4*CTOD$ has been used (7); (e) in a simplified form, the Dodds–Anderson fracture-toughness correction

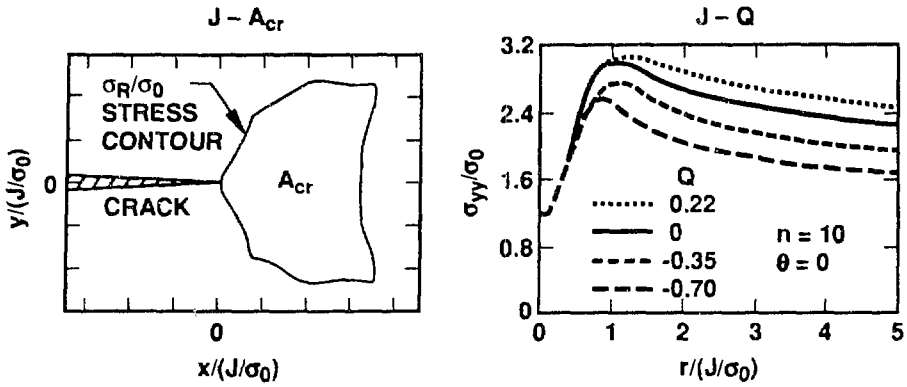

A_{cr} is the area over which stresses exceed the reference stress ratio (σ_R/σ_0) for crack initiation

Q is a parameter characterizing the hydrostatic stresses and therefore the maximum principal stresses ahead of the crack

Fig. 1 Dual-parameter corrections and correlations have been proposed as means for adjusting fracture-toughness data for the effects of crack-tip constraint.

factors can be defined in terms of the constraint-dependent ratio of the applied J-values required to generate the reference opening mode stress value at the selected distance ahead of the crack tip (r); (f) extension of the concept of a reference stress at a specific radius to a reference stress acting over the volume defined by the area contained within a reference stress contour (Acr) in a unit thickness-plate provides a means of reflecting the statistical nature of cleavage initiation in the fracture-toughness process. In practice results obtained using this extension of the concept compare closely with those predicted using the reference stress radius approach (7).

Use of the simplified form of the Dodds–Anderson correction factor approach is illustrated in Fig. 2. Note that the value of "*r*" in the expression $r\sigma_0/J$ remains constant. The critical J-value for

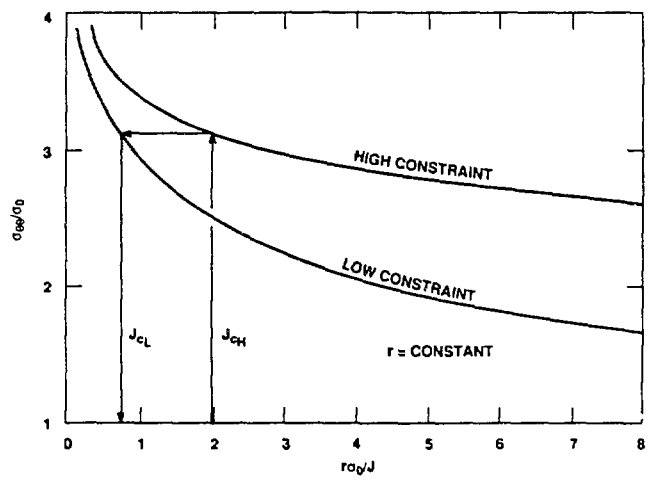

Fig. 2 A simplified form of the Dodds–Anderson correction factor can be used with opening mode stress plots from crack-tip analyses to make J_c predictions for modified constraint configurations.

a low constraint configuration (J_{cl}) can, therefore, be estimated if the critical J for a high constraint configuration (J_{ch}) is known and the crack-tip, opening-mode stress plots are available for both configurations.

The two-parameter (J-Q), fracture-toughness correlation proposed by O'Dowd and Shih characterizes the effects of stress triaxiality on the crack-tip stress field. The HRR crack-tip stress field is used as the basis of comparison for crack-tip stress fields with differing levels of crack-tip stress triaxiality.

In the J-Q fracture-toughness correlation, Q defines the departure of the stress-state dependent opening mode stress distribution on the crack plane from the HRR opening mode stress distribution. Extensive SSY finite-element analysis performed by O'Dowd and Shih indicates that Q remains relatively constant over the region ahead of the crack-tip in which cleavage initiation is postulated to occur. Q can, therefore, be expressed as follows.

$$Q \equiv \frac{\sigma_{yy} - (\sigma_{yy})\mathrm{HRR}}{\sigma_O} \qquad (1)$$

Where σ_{yy} is the crack-tip opening mode stress distribution for a specific constraint condition, (σ_{yy})HRR is the corresponding stress distribution for the HRR constraint condition, and σ_0 is the material yield stress. Q is postulated to remain constant over the crack-tip process zone and is conventionally evaluated at $r = 2J/\sigma_0$.

In physical terms, Q is the difference between the hydrostatic stress associated with the reference HRR crack-tip stress distribution and the crack-tip hydrostatic stress associated with a specific constraint condition. Q is conventionally expressed in a normalized form by dividing the hydrostatic stress increment by the material yield strength. A reduction in constraint relative to the reference HRR constraint condition produces a negative Q-value.

Rice's J-integral (10) sets the size of the zone over which large crack-tip stresses act. Fig. 1(b) shows the crack-tip opening mode stress distribution for a range of constraint conditions characterized by Q. The distance "r" ahead of the crack tip is normalized by dividing by the parameter (J/σ_0). In non-normalized form any one of the curves shown in Fig. 1(b) would appear as a family of curves with the peak on the curve moving further from the crack-tip as J increases.

A fracture prevention margin calculated using a single parameter characterization of fracture-toughness would be expressed as the ratio of the material fracture-toughness to the crack driving force (K_{Ic}/K_I or J_c/J). The equivalent process using the J-Q characterization of fracture-toughness is illustrated in Fig. 3. The single-parameter characterization of fracture-toughness at a particular value of RT_{NDT} is replaced with a J-Q fracture-toughness locus. Given the data scatter inherent to the fracture process, the J-Q locus takes the form of a J-Q data scatter band with upper and lower bounds. Fracture-toughness tests on specimens with varying levels of crack-tip constraint, such as those described later in this paper, are used to generate the data required to define the J-Q locus scatter band.

Elastic-plastic, finite-element analysis of the crack-tip region defines J and Q for each step in the loading sequence. Intersection of the locus of these points with the lower bound of the J-Q fracture-toughness scatter band defines the minimum J and the associated Q for fracture initiation. This value of J can then be compared with J produced by the maximum component loading to determine the fracture prevention margin for the component. Characterization of the J-Q fracture-toughness scatter band in statistical terms permits extension of the concept for use in probabilistic fracture mechanics analyses.

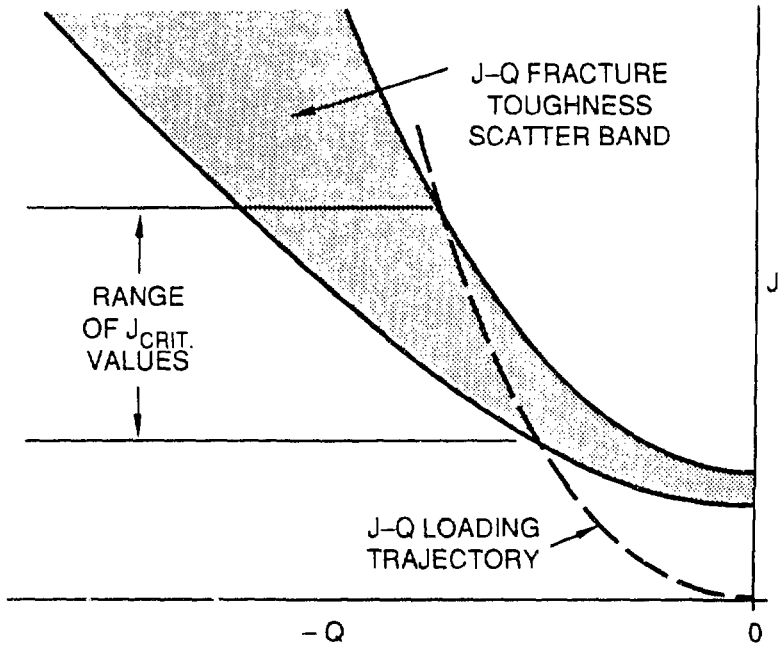

Fig. 3 Intersection of the J-Q loading trajectory for a specific configuration and loading condition with the material J-Q fracture-toughness scatter band defines the range of critical J values

It will be evident from the above discussion of the J-Acr and J-Q dual-parameter concepts that they have much in common. Principles (a) and (b) described above for the J-Acr correction factor concept are equally applicable to the J-Q dual-parameter, fracture-toughness correlation concept. The J-Q concept assumes that Q will remain relatively constant over the process zone and, therefore, does not require that a specific location be selected for a comparison of Q values. It has, however, become customary to use the location defined by $r = 2J/\sigma_0$ for this purpose.

Shallow-Flaw Fracture-Toughness Tests

Fracture-toughness tests have been performed on single-edge, notch-bending (SENB) test specimens using both deep- (a/W = 0.5) and shallow- (a/W = 0.1) flaws (Ref. 11). Beam specimens used in these tests are shown in Fig. 4. The beams were fabricated from A533B material and were nominally 100 mm (4 in.) deep. Use of beams with this depth permitted testing of shallow flaws with depths in the range identified as the critical depth range for PTS analysis. Use of prototypical flaw depths reduced somewhat the uncertainties associated with extrapolation of shallow-flaw, fracture-toughness data for application to full-scale structures (12).

Details of these tests have been extensively reported elsewhere (11, 13, 14), and will not be repeated here. Data from the tests are important to both the ongoing development of dual-parameter, fracture-toughness correlations and the investigation of biaxial loading effects on crack-tip constraint and fracture-toughness. The deep-flaw and shallow-flaw fracture-toughness data generated in these tests were produced using a single material and closely controlled test conditions. Differences between the deep-flaw and shallow-flaw fracture-toughness data obtained can, therefore, be reliably attributed to differences in crack-tip-constraint for the deep and shallow flaws. This attribute permits the data to be used, together with a J-Q analysis of the test specimens and loading conditions, to generate preliminary definitions of the J-Q failure locus scatter band for temperatures ($T\text{-}RT_{NDT}$) investigated in the tests. The shallow-flaw portion of the data base also

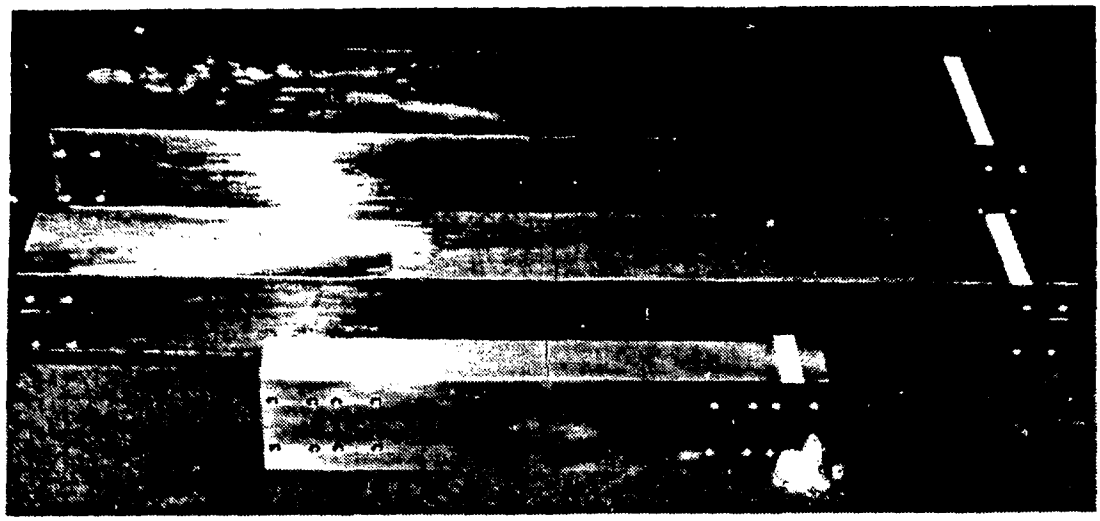

Fig. 4 100 mm deep beams were used in the shallow-flaw test program to permit full-scale testing of surface flaws having depths in the range which PTS analysis has shown to be the controlling range for crack initiation

provides a basis for assessing the effect of biaxial loading on the shallow-flaw, fracture-toughness of A533B material.

Shallow-flaw and deep-flaw fracture-toughness data generated in these tests are plotted in Fig. 5. The data are seen to be grouped into two separate families corresponding to the shallow and deep

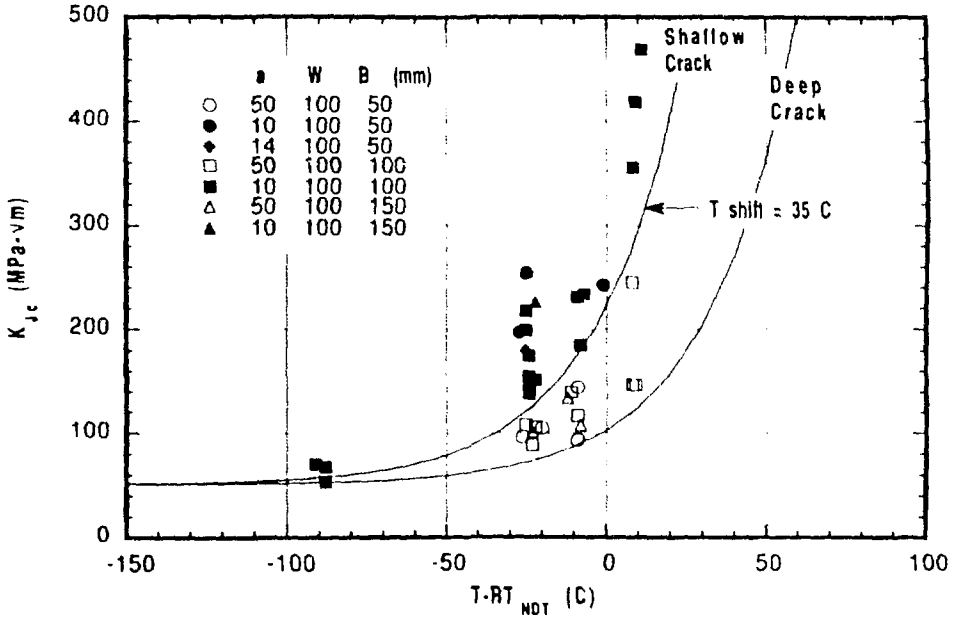

Fig. 5 Data from the shallow-flaw, fracture-toughness testing program show that the shallow-flaw effect produces a substantial increase in toughness at temperatures in the transition region of the fracture-toughness curve.

flaws respectively. Lower bound curves fitted to the data show a 35°C shift in RT_{NDT} between the two data sets. It is appropriate to note that most of the shallow-flaw, fracture-toughness data plotted in Fig. 5 are for a flaw depth of 10 mm (0.4 in.). The shallow-flaw, fracture-toughness would be expected to be flaw-depth dependent, with larger shifts in the RT_{NDT} anticipated as the flaw depth decreases.

Note that the shallow-flaw effect on fracture-toughness is significant in the lower transition range of the fracture-toughness curve, which is the area of the curve important to PTS analysis, but is not significant on the lower-shelf portion of the curve. The transition region of the fracture-toughness curve is a region in which plastic flow at the crack-tip produces crack-tip blunting in advance of cleavage fracture. This result is, therefore, consistent with the concept of reduced crack-tip constraint for shallow flaws producing an associated decrease in hydrostatic stress and increased plastic flow (blunting) prior to cleavage fracture.

Ultimate resolution of the role of the absolute crack-depth "a" and the crack-depth ratio "a/W" in controlling the shallow-flaw, fracture-toughness enhancement effect will require test validation. The HSST Program has initiated the required tests using full-thickness test specimens cut from the wall of a reactor vessel from a canceled nuclear plant. One of the full-thickness test specimens is shown in Fig. 6. These specimens are currently being tested in the 27.10^6 N (6.10^6 lb) test machine at the National Institute of Science and Technology (NIST) under an HSST Program subcontract.

Biaxial Fracture-Toughness Testing Of Shallow Flaws

Biaxial stress fields are produced in a reactor pressure vessel wall by both pressure loading and through-wall temperature gradients. A typical biaxial stress field is shown in Fig. 7, together with a constant depth shallow-surface flaw. One of the principal stresses is seen to be aligned parallel to

Fig. 6 Full thickness shallow- and deep-flaw SENB specimens currently being tested in the 27,000,000 MN (12,000,000 lb) test machine at the National Institute of Standards and Technology.

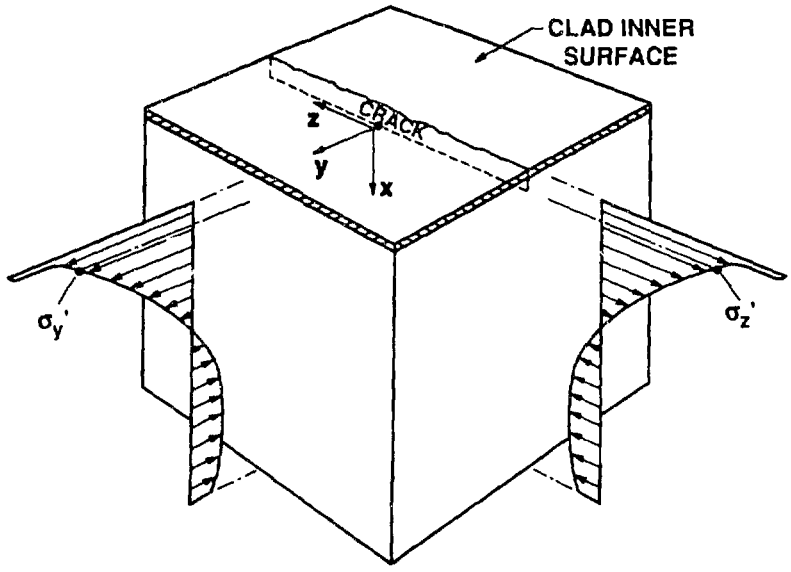

Fig. 7 PTS loading produces biaxial stresses in a reactor vessel wall with one of the principal stresses aligned parallel with the tip of a constant depth shallow-surface flaw.

the crack front. There is no counterpart of this far-field, out-of-plane stress in the shallow-flaw, fracture-toughness tests previously described. The far-field, out-of-plane stress has the potential to increase stress triaxiality (constraint) at the crack-tip and thereby reduce some of the fracture-toughness elevation associated with shallow flaws. The HSST biaxial test Program was instituted to investigate this effect.

Test Specimen Functional Requirements

A number of researchers have investigated the effects of biaxial loading on fracture-toughness (15, 16, 17, 18, 19). These investigations have produced clear indications of a biaxial effect on both cleavage fracture-toughness and on ductile-tearing toughness. They also served to identify some of the difficulties unavoidably associated with biaxial fracture-toughness testing. The specimen size requirement for a meaningful investigation of biaxial loading effects in fracture has emerged as one of the most difficult functional requirements to accommodate. If the specimen size relative to the crack-depth is not adequate, gross plastic deformation can occur in the remaining ligament prior to the initiation of cleavage fracture, making interpretation of the test results difficult.

Increasing the test specimen size will overcome the difficulty outlined above, but at the same time sharply increase the cost of both the test specimen and the test. Increases in the test-specimen size can, therefore, result in testing costs which severely restrict the scope of a testing program. Costs must be tightly controlled in order to permit an adequate investigation of fracture-toughness data scatter under biaxial loading conditions. It follows, therefore, that basic functional requirements for the biaxial fracture-toughness test specimen are (a) low cost, and (b) a configuration, which will minimize departure from elastic behavior in the unbroken ligament up to the instant of fracture.

An equally important functional requirement for the test specimen is that it permits any biaxial effect on shallow-flaw, fracture-toughness to be clearly identified. The test specimen must, therefore, be capable of being loaded in either a uniaxial or a biaxial configuration, with all other test parameters remaining unchanged.

An infinitely long (constant depth) geometry is assumed for all shallow flaws in conformance with the PTS analysis guidelines provided in U.S. NRC Regulatory Guide 1.154 (Ref. 20). Evaluation of flaws discovered during an in-service inspection, and possible future developments of PTS analysis technology, creates a need for data on the fracture-toughness of finite-length shallow surface flaws. A further basic functional requirement for the test specimen design is, therefore, that it be capable of accommodating both of these flaw geometries.

Test Specimen Design

A number of potential test specimen configurations were considered prior to selection of the cruciform design. Several specimen designs were identified which could satisfy the technical elements of the functional requirements. Test specimen cost was a major factor influencing the final selection.

Conceptual features of the cruciform biaxial fracture-toughness test specimen are illustrated in Fig. 8. The specimen design is capable of reproducing a linear approximation of the nonlinear biaxial stress distribution shown in Fig. 7. The cruciform design, coupled with a statically determinate load reaction system, permits the specimen to be loaded in either uniaxial (4 point

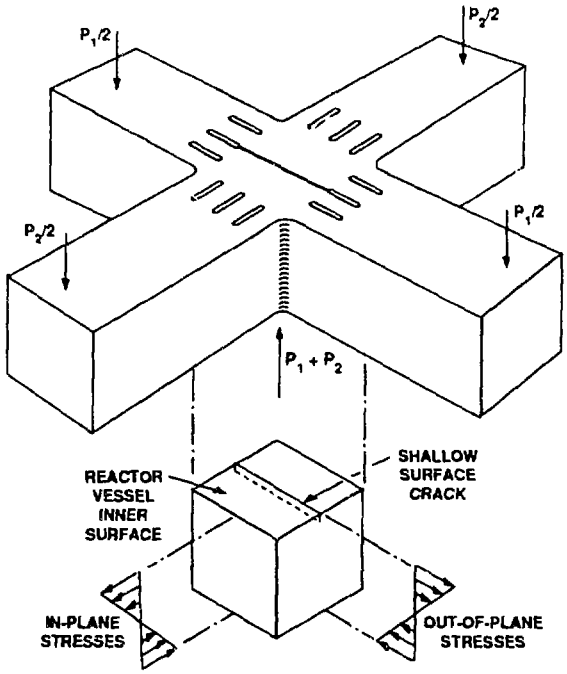

Fig. 8 Conceptual features of the cruciform shallow-flaw, biaxial fracture-toughness test specimen

bending) or biaxial (8 point bending) configurations. Tests of nominally identical specimens can thus be performed with the level of stress biaxiality as the only test variable. Details of the statically determinate load reaction system are given in Fig. 9.

Load diffusion control slots permit the maintenance of a reasonably uniform biaxial stress field within the test section of the specimen. The uniform depth shallow-flaw terminates at the central

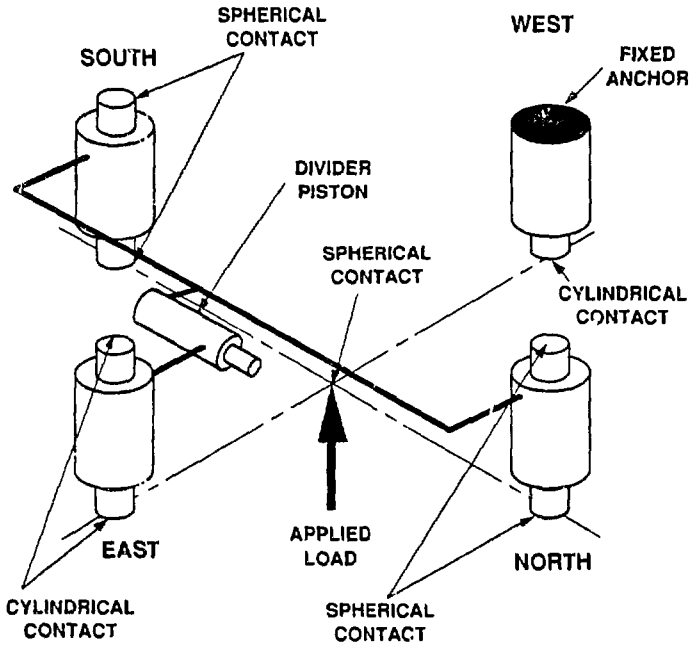

Fig. 9 Hydraulically coupled passive load-reaction jacks assure that the test specimen loading is statically determinate. A divider piston in the hydraulic coupling line provides control of the beam loading ratio.

load diffusion control slots, thereby simulating an infinitely long flaw. Control of the differential length of the central load diffusion control slots relative to the lengths of the outer slots is used to eliminate unacceptable stress concentrations at the ends of the crack.

The central block of the cruciform specimen is the only portion fabricated from fully characterized test material. The load diffusion control slots are machined in both the test block and the reusable arms using a numerically controlled electro-discharge machining (EDM) process. The crack starter slot is machined at the same time. A completed central block is shown in Fig. 10.

Longitudinal arms are attached using a low-heat input electron beam (EB) welding procedure prior to fatigue precracking the specimen in four point uniaxial bending. A mechanical machining operation is used to remove any EDM embrittled material and any fatigue-crack growth irregularities from the central load diffusion control slots at the ends of the crack. Attachment of the transverse load arms by EB welding completes the fabrication process. The resulting test specimen, which is shown in Fig. 11, meets all of the functional requirements and is considerably lower in cost and material requirements than any of the alternate designs evaluated.

Test Specimen Analysis

A three-dimensional, finite-element model of cruciform specimen, incorporating a highly refined representation of the crack-tip region, was used for this analysis. Essential features of the model are shown in Fig. 12. The model has 3890 isoparametric brick elements. For the crack-tip field analysis, the crack-tip region is modeled using collapsed prism elements arranged in a fan configuration. The analyses were run using the ABAQUS (Ref. 21) computer program and a piecewise representation of the material elastic-plastic, stress-strain properties. Further details of the analysis procedure can be found in Ref. 22.

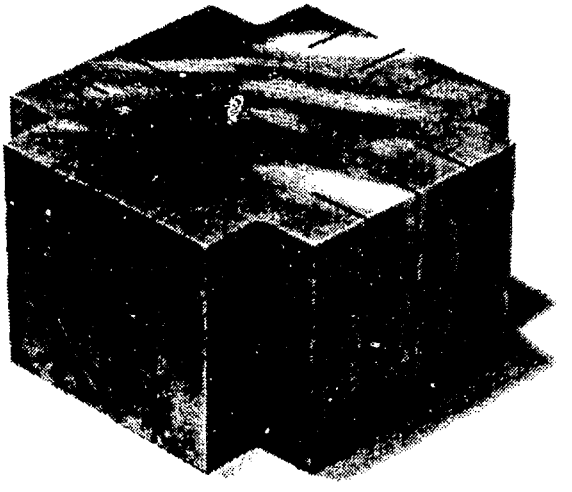

Fig. 10 The differential load-diffusion control slot lengths used to control stress concentrations at the slot-crack interface can be seen in the completed central block.

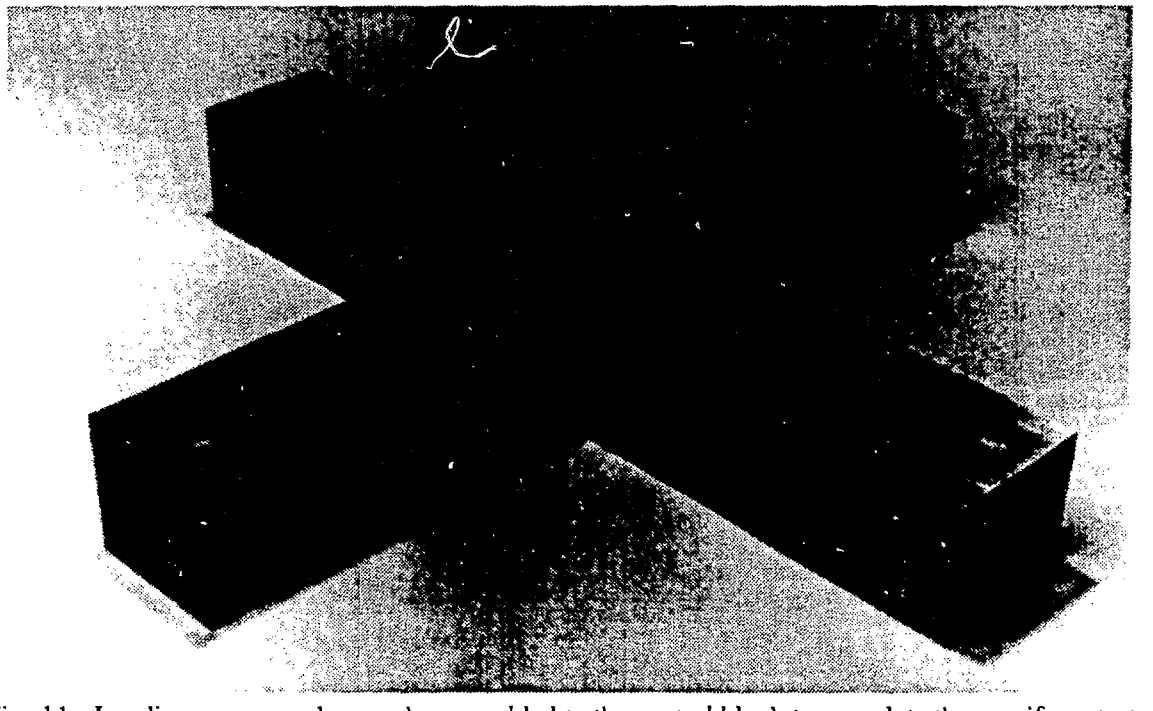

Fig. 11 Loading arms are electron-beam welded to the central block to complete the cruciform test specimen.

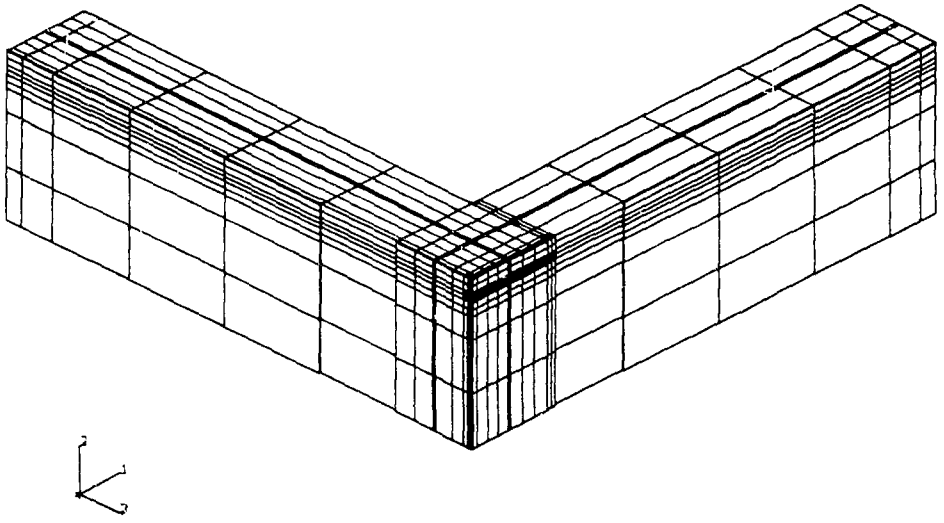

Fig. 12 A cruciform model incorporating a highly refined crack-tip region was used for the local crack-tip field analysis.

Validation checks were performed on the analysis model before it was used to interpret the test data. Results from one of the most stringent of those checks are shown in Fig. 13. Load vs crack-mouth-opening displacement (CMOD) predictions from the analysis were required to match test values for this parameter set over the full range of test values. Iterative adjustments were made to the material stress-strain representation to achieve the close match between analytical predictions and test results shown in Fig. 13.

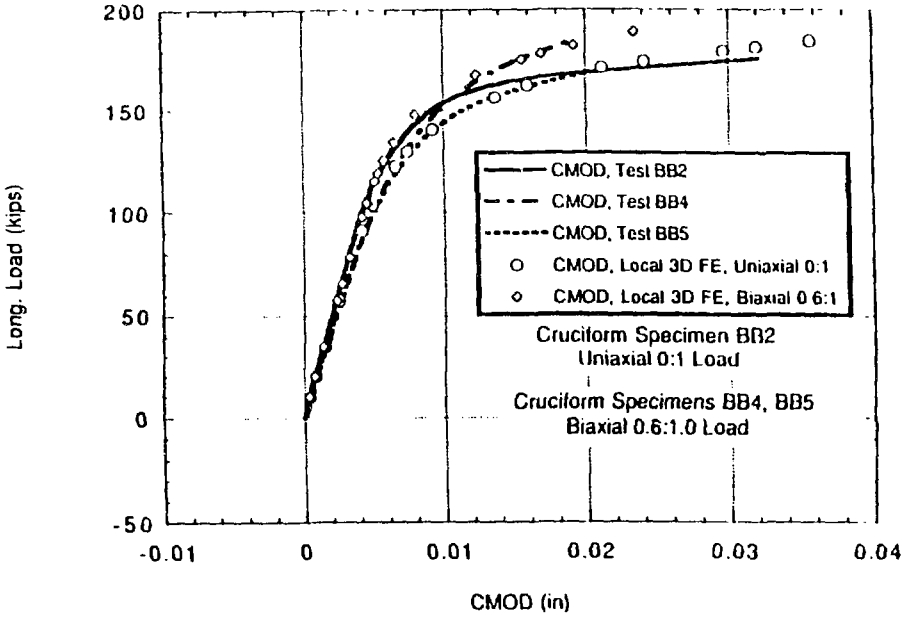

Fig. 13 Analysis model predictions match closely the load vs CMOD results obtained in the uniaxial and biaxial tests.

Two schemes for estimating J_c from the biaxial test results were evaluated by Theiss et al. in Ref. 23. The methods are based on estimating the energy deposited in the crack-tip material using (a) the area under the load vs load-line displacement curve, and (b) the area under the load vs CMOD curve. The latter scheme was considered the more accurate of the two because the CMOD measurement is made close to the crack tip. The load vs CMOD curve provides, therefore, a more sensitive measure of the energy deposited in the crack-tip material.

The applied J integral at fracture (J_c) is expressed in terms of elastic and plastic elements of the load vs CMOD curve in equation 2.

$$J_c = J_{el} + J_{pl} \qquad (2)$$

Where

J_{el} = elastic contribution to $J_c = K_c^2(1 - \nu^2)/E$
K_c = applied stress intensity factor
ν = Poisson's ratio
E = Young's modulus

J_{pl} = plastic contribution to $J_c = \eta_{pl}^c U_{pl}^c B(W - a)]$

η_{pl}^c = dimensionless factor determined by analysis and relating the plastic area under the load vs CMOD curve to J_{pl}. Note that η_{pl}^c is stress-state dependent.

U_{pl}^c = plastic portion of the area under the load vs CMOD curve
a = crack depth
W = test specimen width (depth)
B = test specimen thickness

Output from the analysis also included a definition of the applied crack-tip J for all points along the crack-front. One set of these results is shown in Fig. 14 in terms of the more familiar K_J. Biaxial loading is seen to produce a nonuniform distribution of K_J along the crack-front, with the departure from linearity increasing as specimen is loaded further into the regime of nonlinear behavior. This trend makes consideration of the crack initiation site necessary to an accurate interpretation of the test data.

Plots of the Von Mises equivalent stress distribution over the test specimen ligament are shown in Fig. 15 for uniaxial and biaxial loading conditions. Both plots represent conditions at failure as determined in the tests. Note that the Von Mises equivalent stress exceeds the material yield stress by a small amount over much of the ligament in the uniaxial loading case. Biaxial loading, in contrast, results in the ligament remaining elastic. This result could have been anticipated by imposing an out-of-plane stress on the published stress distributions for notched bars (Ref. 24). One consequence of biaxial loading is, therefore, to increase crack-tip constraint by suppressing large-scale plastic deformation of material in the immediate vicinity of the crack.

Results from the crack-tip field portion of the analysis are shown in Fig. 16. The curves in Fig. 16 show the opening mode stress distribution ahead of the crack for both uniaxial and biaxial loading, together with the reference (high constraint) opening mode stress distribution. It is evident from these curves that Q does not remain constant with distance ahead of the crack tip for the case of uniaxial loading. Biaxial loading, in contrast, results in relatively constant values of Q for $r > 2J/\sigma_0$. This observed trend for uniaxial loading is incompatible with one of the postulates upon which the J-Q fracture-toughness correlation is based, indicating a need for some further development of that correlation. The Dodds–Anderson correction factor approach is not

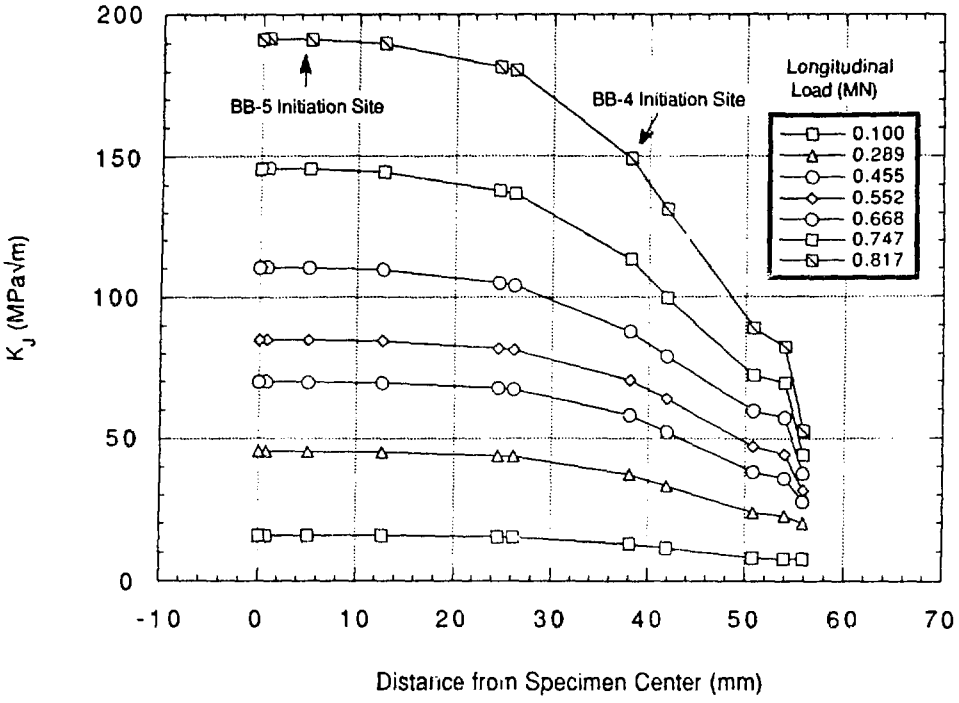

Fig. 14 Variation of K_J along the crack front for a 0.6:1.0 biaxial loading condition.

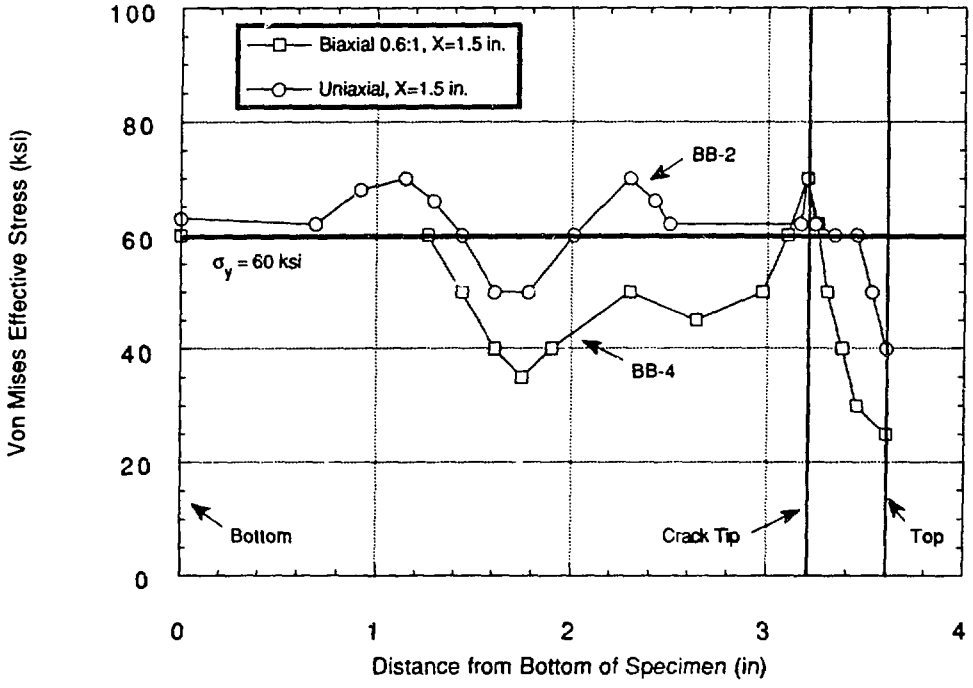

Fig. 15 Ligament stresses at fracture exceed the yield stress under uniaxial loading but remain elastic under biaxial loading.

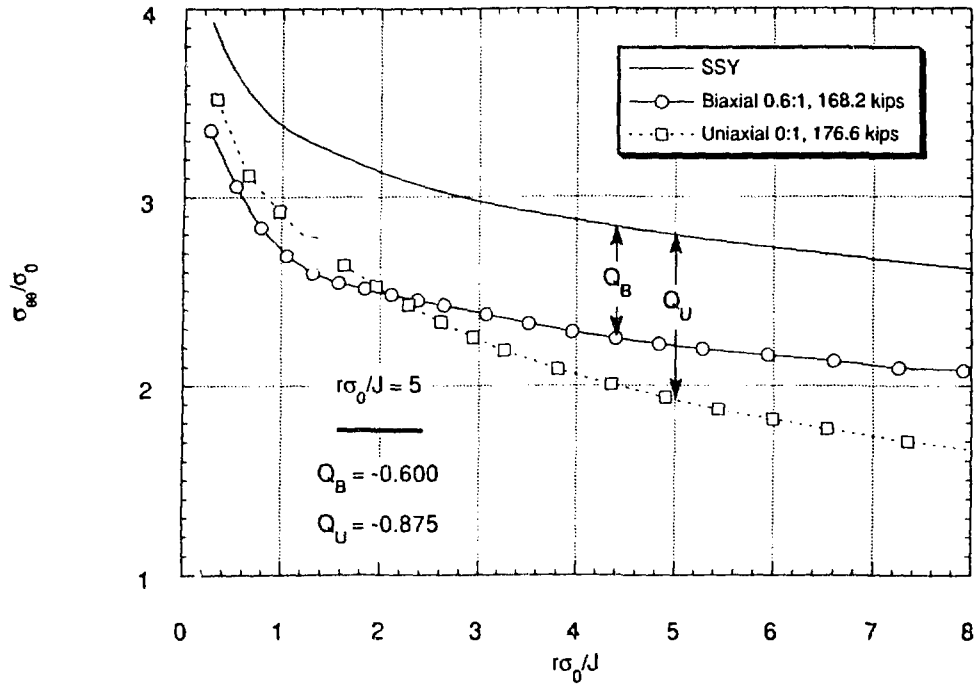

Fig. 16 Stress biaxiality improves the uniformity of the Q-stress field relative to the Q-field obtained with uniaxial loading.

compromised by the results illustrated in Fig. 16 because it is not based upon the assumption of a uniform Q-stress field ahead of the crack tip.

Test Results

The first requirement for the test program was to demonstrate that the configuration of the crack and the load-diffusion control (LDC) slots would produce crack initiation remote from the intersection of these two features. Satisfaction of this requirement was essential to assure that the measured test results were a true reflection of the influence of the test parameters on shallow-flaw, fracture-toughness and were not influenced by stress concentration effects at the ends of the LDC slots. The requirement was found easier to satisfy under uniaxial loading than biaxial loading. The configuration of the crack-geometry and LDC slot geometry finally selected was capable of assuring crack initiation away from the intersection under both uniaxial and biaxial loading. Figure 17 shows a fracture surface from one of the biaxial tests. The river patterns in Fig 17 show the fracture to have initiated close to the mid point of the crack.

Extensive calibration of the test fixture was undertaken prior to the initiation of testing. A dummy cruciform specimen fitted with multiple strain gauges was used in this phase of the program. Results demonstrated that the statically determinate load reaction system was working as planned. Pretest preparations culminated in a test readiness review, in which an independent body of fracture mechanics experts found the test program ready for implementation.

Clip gauges and displacement transducers were used to measure CMOD and load-line displacement (LLD), respectively, as a function of the applied load. Test temperatures were selected to be in the lower transition region of the shallow-flaw, fracture-toughness curve. This is the area of the fracture-toughness curve of particular interest in determining the effect of biaxial loading on ΔRT_{NDT}.

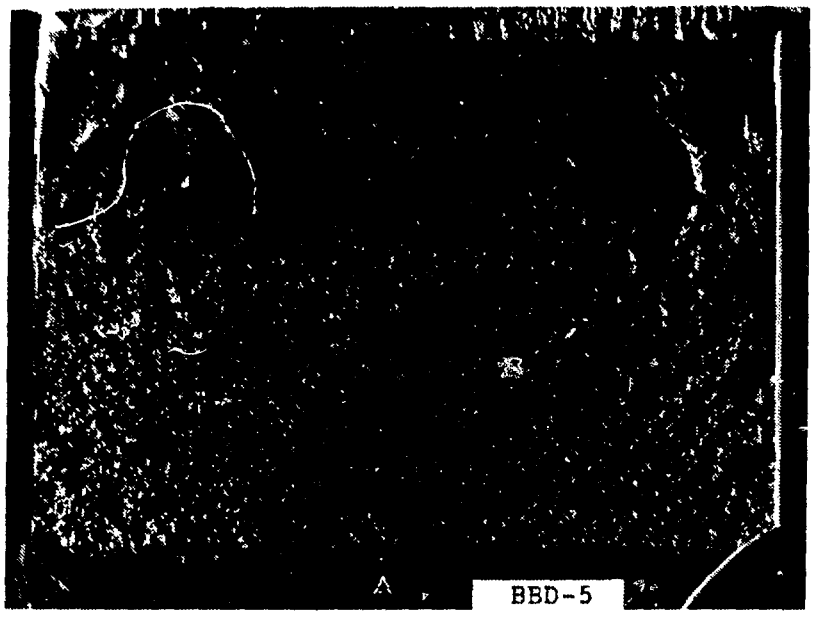

Fig. 17 Cleavage fracture initiated in the mid-thickness of the biaxial test specimen, remote from any structural discontinuities.

Load vs CMOD curves generated in three of the four valid tests completed to date were shown in Fig. 13. Note that the measured CMOD at failure is remarkably similar for the two biaxial tests. Biaxial loading substantially reduces the CMOD at failure when compared with the uniaxial loading result.

Test values for K_{Jc} are shown in Fig 18, superimposed on data from the shallow-flaw and deep-flaw SENB tests. The cruciform beam data plotted in Fig 18 corresponds with the point on the crack front at which post-test examination showed the crack to have initiated. The cruciform specimen tested under uniaxial loading produced a fracture-toughness close to the lower bound of the fracture-toughness scatter band from the shallow-flaw SENB tests. Biaxial loading of the cruciform specimen produced two results below the lower bound of results from the shallow-flaw SENB data set. The two data points from biaxial loading tests on the cruciform specimen are seen to be closely matched.

Test data generated to date are consistent with expectations for the biaxial tests. Biaxial loading appears to reduce K_{Jc} below the values associated with shallow flaws, but not down to the lower bound values associated with highly constrained deep flaws. There are also indications that biaxial loading may reduce the scatter of shallow-flaw, fracture-toughness data. The biaxial testing program is, however, in its infancy, and the amount of data currently available from the program is not sufficient to support an assessment of biaxial loading effects on shallow-flaw, fracture-toughness at this time.

Test Data Interpretation

The objective in this section is to illustrate the practical application of constraint effects technology to the safety assessment of an irradiation-embrittled reactor pressure vessel. Fracture-toughness data reflecting the effect of varying levels of crack-tip constraint are essential input to such a safety assessment. At this time the amount of data available from the biaxial testing program is too small to support a safety assessment. This example, therefore, utilizes data from the previously

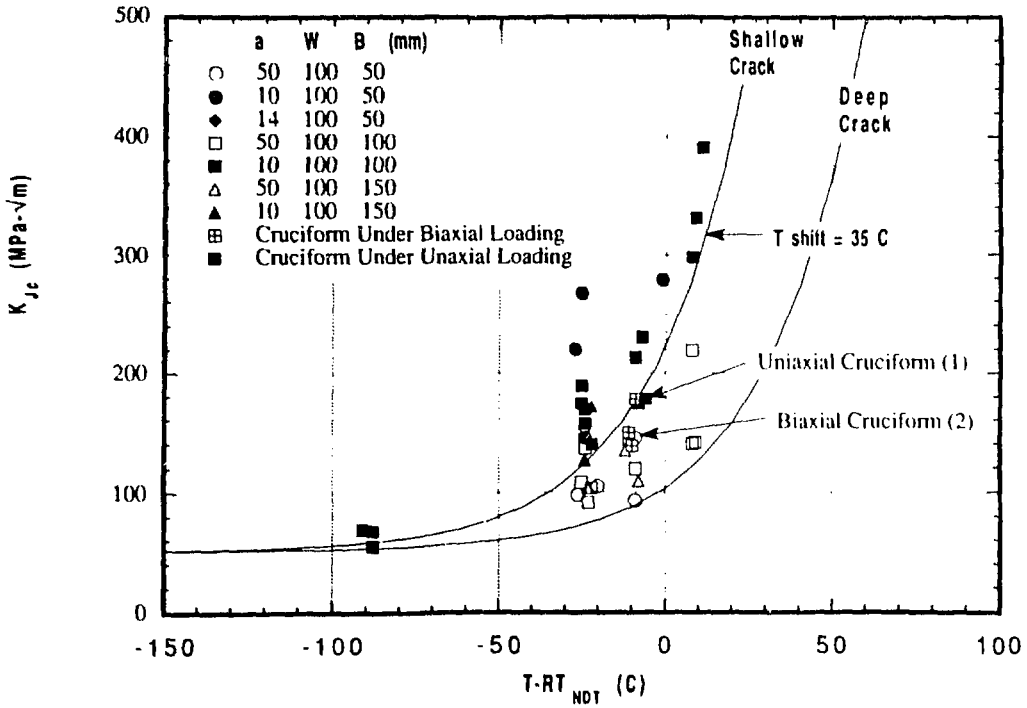

Fig. 18 Biaxial loading resulted in shallow-flaw, fracture-toughness values below the lower bound values obtained under uniaxial loading.

completed HSST shallow-flaw tests on SENB specimens. Data used in this assessment were taken from Ref. 11. The data set of Ref. 11 cover two constraint configurations. These are deep flaws with an a/W of 0.5 and shallow flaws with an a/W ratio of 0.1. Prof. R. Dodds has performed a J-Q analysis of these test specimens under an HSST Program subcontract. J-Q trajectories for both the shallow- and deep-flaw beams are shown in Fig. 19, together with a J-Q loading trajectory from one of the HSST Program wide-plate tests (Ref. 25).

Fracture-toughness data from each of the test series are shown in Fig. 19, superimposed on the appropriate J-Q loading trajectory. Upper and lower bounds to the resulting J-Q scatter band are represented in Fig. 19 by straight lines. This representation reflects the fact that only two constraint-effects data sets are available at this time. A more accurate definition of the bounds of the J-Q failure locus scatter band will be possible when more data become available. The data shown in Fig. 19 were all generated at the same test temperature (–10°C). A similar data set exists for tests performed at –25°C.

The lower bound to the J-Q failure locus scatter band defines the minimum anticipated increase in fracture-toughness over the reference high-constraint toughness as the constraint parameter Q decreases from the reference high constraint value ($Q = 0$). Minimum anticipated fracture-toughness increases due to loss of crack-tip constraint are plotted in Fig. 20(a) for each of the test temperatures. Note that fracture-toughness in Fig. 20(a) has been expressed in terms of K_{Jc} rather than J_c. This was done to permit the final result from this example to be expressed in terms of the fracture-toughness units currently in use in RPV safety assessments.

The plots of Fig. 20(a) can now be used to predict the lower-bound, fracture-toughness curve for a given crack-tip constraint condition. In the example given, a constraint loss characterized by Q = –0.6 was used. Predicted fracture-toughness increases for Q = –0.6 are 34 MPa$\sqrt{m}$ at T-RT$_{NDT}$ =

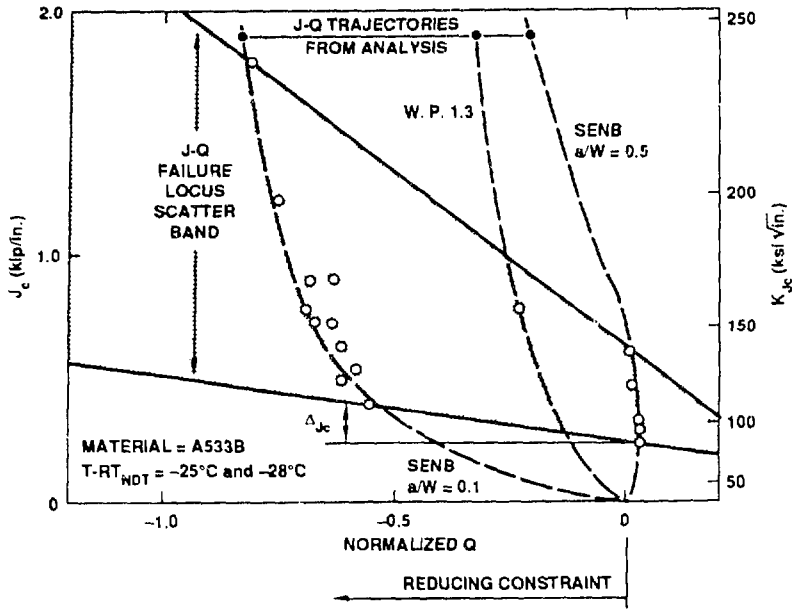

Fig. 19 The J-Q failure locus scatter band shows increased toughness and increased data scatter as the crack-tip constraint decreases (Q becomes more negative).

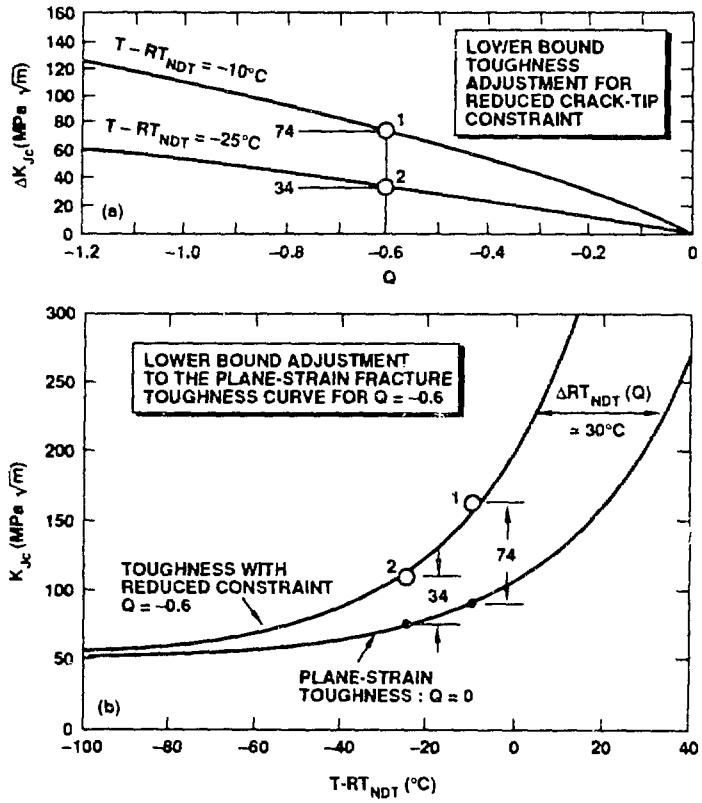

Fig 20. A fracture-toughness curve for a reduced crack-tip constraint condition can be generated using the plane-strain, fracture-toughness curve and the J-Q failure locus envelope.

$-25°C$ and 74 MPa$\sqrt{m}$ at T-RT_{NDT} = $-10°C$. These values are now transferred to Fig. 20 (b) where they are shown plotted as increases over the base material fracture-toughness curve. Transition of the base material curve to the left, such that it passes as closely as possible through the two data points, completes the process. The resulting curve represents the lower bound fracture-toughness for a given level of crack-tip constraint, a constraint level characterized by $Q = -0.6$ in this example.

In a practical application of the J-Q methodology, lower bound fracture-toughness curves could be produced for a range of crack-tip constraint conditions. An analysis of the crack-tip stress fields would, however, be required to determine the constraint condition appropriate for a given geometry and loading condition. It is possible, however, that J-Q analyses for a range of geometry and loading conditions commonly encountered in RPV safety analyses could be performed and the resulting J-Q loading trajectories documented. This approach could eliminate the need for repeated performance of the relatively expensive crack-tip field analysis.

The above example dealt with application of J-Q constraint-effects technology to a deterministic analysis of RPV safety. The technology could also be applied to the probabilistic analysis of RPV safety. The impact of J-Q technology on a probabilistic analysis would be expected to be greater than the impact on a deterministic analysis. This is so because both the mean value of the fracture-toughness scatter band and the width of the scatter band increase more rapidly with loss of crack-tip constraint than does the lower bound fracture-toughness. These trends are evident in the J-Q fracture-toughness scatter band illustrated in Fig. 19.

Verification Checks

Fractographic examination of the broken test specimens provides information on the location of the cleavage initiation sites. Initiation site assumptions are built into the J-Q constraint effects technology. A comparison of the initiation site locations from the test specimens with the initiation site assumptions in the J-Q technology is used as a verification check on the technology.

Opening mode stress plots for the cruciform specimen in both uniaxial and biaxial loading are shown, together with the opening mode stress plot for a high constraint configuration, in Fig. 21(a). These plots were produced in a finite-strain (large-strain) analysis and, therefore, show a downward trend near the crack tip because of the loss of stress triaxiality in material adjacent to the free surface of the blunted crack tip. Cleavage initiation site data from the fractographic examination of SENB and biaxial specimens tested at a range of temperatures are shown in Fig. 21(b). These plots were produced in a finite-strain (large-strain) analysis and, therefore, show a downward trend near the crack tip because of the loss of stress triaxiality in material adjacent to the free surface of the blunted crack tip. Many of the cleavage initiation site locations are located to the left of the peak on the opening mode stress plots. Locations to the left of the peak of the opening mode stress plots experience a falling opening mode stress as the applied J increases. Experience with warm prestressing indicates that cleavage fracture is unlikely to initiate under conditions of decreasing opening mode stresses. At first sight the analysis results and data of Fig. 21 would appear to call into question the basic assumptions inherent to the J-Q technology. On closer examination, however, the basic question appears to lay with the adequacy of the analytical model used to generate the opening mode stress plots.

The analytical model represents a stationary crack. With such a model, crack-tip blunting increases continuously as the applied J increases. In reality, however, tearing would initiate at some point in the loading cycle for tests conducted at temperatures in the transition range. The primary effect of tearing would be to resharpen the previously blunted crack tip. Resharpening of the crack tip would have the effect of moving the peaks of the opening mode stress plots further to the left. Conceptually, this adjustment could eliminate the incompatibility shown in Fig. 21 between analysis and test results.

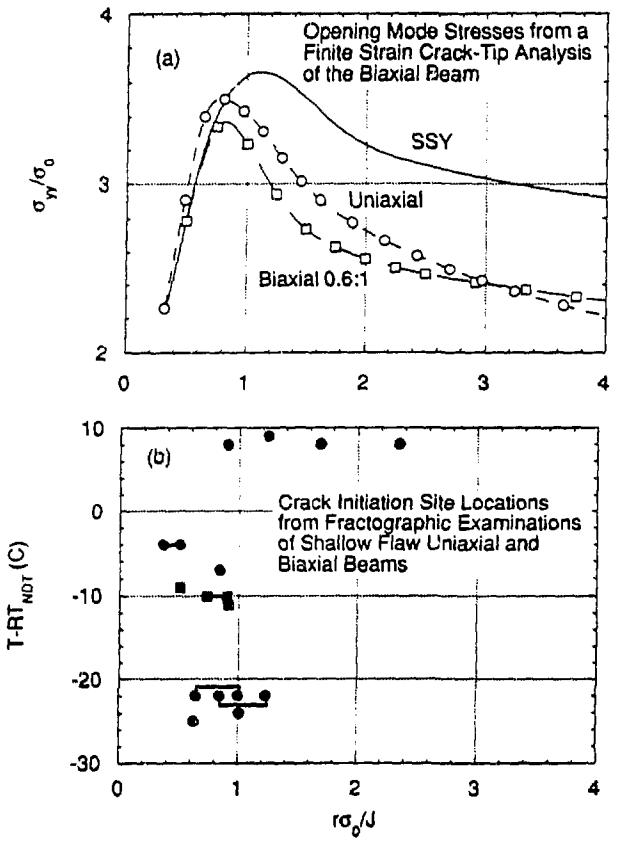

Fig 21. Additional refinement to the crack-tip stress field analysis model appears to be required to reconcile analysis predictions with fractography results.

The analysis model refinement required is one which permits the representation of precleavage tearing. A number of fracture research centers in Europe have had success in developing precleavage tearing models using the critical stress for void formation as defined by the Beremin group and either the Rousselier or Gurson yield models (26, 27, 28). The yield functions take into account the fact that only biaxial stresses can exist at the surface of internal voids. Because of this, application of a hydrostatic stress can result in a plastic volume change. A recent application of this technology by Dr. Dietmar Klingbeil of Bundesanstalt für Materialforschhung und Prufung (BAM), Berlin, Germany, demonstrated that (a) the crack-tip stress field becomes stationary after a relatively small amount of ductile tearing, and (b) the effect of tearing is to "resharpen" the previously blunted crack tip (Ref. 29).

The curves of Fig. 21(a) make it clear that Q cannot be treated as a spatially invariant parameter when, as in the uniaxial loading curve, the overall section and crack-tip plastic stress fields interact. A further question on the selection of the appropriate value for Q derives from the work of Heerens and Read (Ref. 30). They showed, for a low alloy steel tested at –60°C, that the cleavage initiation sites were at the maximum opening mode stress location. A case can, therefore, be made for defining Q as the normalized difference in peak stresses from opening mode stress plots for the reference high constraint configuration and a lower constraint application. It can be seen from the plots of Fig. 21(a) that the value of Q derived using this definition would be considerably smaller than that derived from the "uniform Q-field" definition.

Interim Conclusions

Crack-tip constraint effects of shallow flaws and biaxial loading influence both fracture-toughness and the width of the fracture-toughness scatter band. This influence can have a significant impact on the outcome of an RPV safety analysis.

Dual-parameter (J-Q and J-Acr) fracture-toughness correlations and corrections show promise as a practical means for introducing the effects of crack-tip constraint into reactor pressure vessel safety assessments. Additional refinement of the analysis models used to define crack-tip stress fields appears to be necessary in order to resolve discrepancies between analytical predictions and fractographic data on cleavage initiation sites. Inclusion of precleavage tearing effects into the analysis model appears to have the potential to resolve the observed discrepancies.

Development and validation of technology for the quantitative assessment of crack-tip constraint effects on fracture-toughness is essential to the future utilization of miniature fracture-toughness surveillance specimens.

References

1. R. O. Ritchie, J. F. Knott, and J. R. Rice, "On the Relationship Between Critical Tensile Stress and Fracture Toughness in Mild Steel," *J. Mech. Phys. Solids* 21, 395–410 (1973).

2. G. R. Irwin, "Analysis of Stresses and Strains Near the End of a Crack Traversing a Plate," *American Society of Mechanical Engineers*, Journal of Applied Mechanics, September 1957, pp. 361–364.

3. J. Hutchinson, "Singular Behavior at the End of a Tensile Crack in a Hardening Material," *J. Mech. Phys. Solids* 16, 13–31 (1968).

4. J. R. Rice and G. F. Rosengren, "Plane-Strain Deformation Near a Crack Tip in a Power-Law Hardening Material," *J. Mech. Phys. Solids* 16, 1–12 (1968).

5. *American Society for Testing and Materials Standard No. E399–90*, "Standard Test Method for Plane-Strain Fracture Toughness of Metallic Materials" (1990).

6. T. R. Mager, Westinghouse Electric Corp., "Heavy-Section Steel Technology Program Technical Report No. 10: Fracture Toughness Characterization Study of A533, Grade B, Class 1 Steel," WCAP-7578, October 1970.

7. R. H. Dodds, Jr., T. L. Anderson, and M. T. Kirk, "A Framework to Correlate a/W Ratio Effects on Elastic-Plastic Fracture Toughness (J_c)," *International Journal of Fracture* 48: 1–22, (1991).

8. N. P. O'Dowd and C. F. Shih, "Family of Crack-Tip Fields Characterized by a Triaxiality Parameter: Part I—Structure of Fields," *J. Mech. Phys. Solids* 39, 989–1015 (1991).

9. N. P. O'Dowd and C. F. Shih, *Two-Parameter Fracture Mechanics: Theory and Applications*, USNRC Report NUREG/CR-5958 (CDNSWC/SME–CR–16–92), Oak Ridge National Lab., Oak Ridge, TN, February 1993.

10. J. R. Rice, "A Path Independent Integral and the Approximate Analysis of Strain Concentrations by Notches and Cracks," *Journal of Applied Mechanics*, Vol. 35, pp. 379–386.

11. T. J. Theiss and D. K. M. Shum, *Experimental and Analytical Investigation of the Shallow-Flaw Effect in Reactor Pressure Vessels*, USNRC Report NUREG/CR-5886 (ORNL/TM-12115), Oak Ridge National Lab., Oak Ridge, TN, July 1992.

12. M. T. Kirk, K. C. Koppenhoefer, and C. F. Shih, "Effect of Constraint on Specimen Dimensions Needed to Obtain Structurally Relevant Toughness Measures," *Constraint Effects in Fracture, ASTM STP 1171*, pp. 79–103, March 1993.

13. T. J. Theiss, W. J. McAfee, B. R. Bass, J. W. Bryson, and M. C. Rao, "Preliminary Results from Biaxial Shallow-Flaw Fracture Toughness Tests on Reactor Pressure Vessel Steel," *ASME PVP*, Vol. 250, pp. 271–281, July 1993.

14. B. R. Bass, J. W. Bryson, W. E. Pennell, and T. J. Theiss, "Determination of Out-of-Plane Biaxial Stress Effects on Fracture Toughness for Shallow Surface Cracks in Reactor Pressure Vessel Steels," *ASME PVP*, Vol. 250, pp. 257–269, July 1993.

15. D. Aurich, R. Helms, P. Schmidt, H. Veith, J. Ziebs, "The Influence of the Stress State on K_{Ic}," *Transactions of the Fourth International Conference on Structural Mechanics in Reactor Technology*, Vol. G, August 1977.

16. D. Aurich, W. Brocks, R. Jordan, J. Olschewski, H. Veith, and J. Ziebs, "The Influence of Multiaxial Stress States on Characteristic Parameters for Cleavage Fracture in the Elastic-Plastic Range," *Proceedings of the International Applied Fracture Mechanics to Materials and Structures*, 1984.

17. D. Aurich and E. Sommer, "The Effect of Constraint on Elastic-Plastic Fracture," *Metalle und Metallkonstruktionen*, Steel Research 59, No. 8, pp. 358–367, 1988.

18. H. Clausmeyer, K. Kussmaul, and E. Roos, "Influence of Stress State on the Failure Behavior of Cracked Components Made of Steel," *Applied Mechanics Rev*, Vol. 44, No. 2, February 1991.

19. S. J. Garwood, "The Significance of Biaxial Loading on the Fracture Performance of a Pressure Vessel Steel," *Pressure Vessel Integrity*, PVP-Vol. 213, MPC-Vol. 32, June 23–27, 1991.

20. Office of U.S. Nuclear Regulatory Research, U.S. Nuclear Regulatory Commission Regulatory Guide 1.154 (Task SI 502-4), Format and Content of Plant-Specific Pressurized Thermal Shock Safety Analysis Reports for Pressurized Water Reactors, January 1987.

21. ABAQUS Theory Manual, Version 4–8, Hibbitt, Karlson, and Sorensen, Inc., Providence, R. I., 1989.

22. B. R. Bass, J. W. Bryson, T. J. Theiss, and M. C. Rao, *Biaxial Loading and Shallow-Flaw Effects on Crack-Tip Constraint and Fracture Toughness*, USNRC Report NUREG/CR-6132 (ORNL/TM-12498), to be published in November 1993.

23. J. A. Hendrickson, D. S. Wood, and D. S. Clark, "The Initiation of Brittle Fracture in Mild Steel," Trans., ASM (50), 1958, pp. 656.

24. T. J. Theiss, B. R. Bass, J. W. Bryson, W. J. McAfee, R. K. Nanstad, W. E. Pennell, and M. C. Rao, *Initial Results of the Influence of Biaxial Loading on Fracture Toughness*, USNRC Report NUREG/CR-6036 (ORNL/TM-12349), Oak Ridge National Lab., Oak Ridge, TN, June 1993.

25. D. J. Naus, B. R. Bass, C. E. Pugh, R. K. Nanstad, J. G. Merkle, W. R. Corwin, G. C. Robinson, *Crack-Arrest Behavior in SEN Wide Plates of Quenched and Tempered A533 Grade B Steel Tested Under Nonisothermal Conditions*, USNRC Report NUREG/CR-4930 (ORNL-6388), Oak Ridge National Lab., Oak Ridge, TN, August 1987.

26. K. Kussmaul, M. Seidenfuss, and U. Eisele, "On the Applicability of Damage Models for the Description of the Failure Behavior of Ductile Steels," presented at the International Conference on Fracture, Kiev, Ukraine, June 1993.

27. G. Rousselier, "Ductile Fracture Models and Their Potential in Local Approach of Fracture," Nuclear Engineering and Design 105, North-Holland, Amsterdam, pp. 111, 1987.

28. A. H. Sherry, "Elastic-Plastic, Finite-Element Analysis of Circumferentially Notched Tensile Specimen," AEA Thermal Reactor Services, AEA Technology, January 1991.

29. W. E. Pennell and W. R. Corwin, "ORNL Foreign Trip Report," ORNL/FTR-4673, July 1993.

30. J. Heerens and D. T. Read, "Fracture Behavior of a Pressure Vessel Steel in the Ductile-to-Brittle Transition Region," NISTIR 88-3099, National Institute for Standards and Technology, Boulder, CO, December 1988.